Investigation of Coded Source Neutron Imaging at the North Carolina State University PULSTAR Reactor

Ziyu Xiao, Kaushal K. Mishra, Ayman I. Hawari
Hassina Z. Bilheux, Philip R. Bingham, and Kenneth W. Tobin, Jr.

Abstract–A neutron imaging facility is located on beam-tube #5 of the 1-MWth PULSTAR reactor at the North Carolina State University. An investigation has been initiated to explore the application of coded imaging techniques at the facility. Coded imaging uses a mosaic of pinholes to encode an aperture, thus generating an encoded image of the object at the detector. To reconstruct the image recorded by the detector, corresponding decoding patterns are used. The optimized design of coded masks is critical for the performance of this technique and will depend on the characteristics of the imaging beam. In this work, Monte Carlo (MCNP) simulations were utilized to explore the needed modifications to the PULSTAR thermal neutron beam to support coded imaging techniques. In addition, an assessment of coded mask design has been performed. The simulations indicated that a 12 inch single crystal sapphire filter is suited for such an application at the PULSTAR beam in terms of maximizing flux with good neutron-to-gamma ratio. Computational simulations demonstrate the feasibility of correlation reconstruction methods on neutron transmission imaging. A gadolinium aperture with thickness of 500 μm was used to construct the mask using a 38 × 34 URA pattern. A test experiment using such a URA design has been conducted and the point spread function of the system has been measured.

I. INTRODUCTION

THE concepts of coded imaging techniques were first introduced and implemented in the field of astronomy in the early 1960s, as coded aperture imaging (CAI). Currently CAI has been well developed in the applications for both far-field and near-field problems, such as X-ray astronomy, and biomedical imaging.

Z. Xiao is with the Department of Nuclear Engineering, North Carolina State University, Raleigh, NC, USA. (telephone: 919-513-4465, e-mail: zxiao@ncsu.edu).

K. K. Mishra is with the Department of Nuclear Engineering, North Carolina State University, Raleigh, NC, USA. (telephone: 919-513-4465, e-mail: kkmishra@ncsu.edu).

Ayman I. Hawari is with the Department of Nuclear Engineering, North Carolina State University, Raleigh, NC, USA. (telephone: 919-515-4598, e-mail: ayman.hawari@ncsu.edu).

Hassina Z. Bilheux is with Neutron Scattering Division, Oak Ridge National Laboratory, Oak Ridge, TN, USA. (telephone: 865-241-7534, e-mail: bilheuxhn@ornl.gov).

Philip R. Bingham is with Measurement Science and Systems Engineering Division, Oak Ridge National Laboratory, Oak Ridge, TN, USA. (telephone: 865-574-5680, e-mail: binghampr@ornl.gov).

Kenneth W. Tobin, Jr. is with Oak Ridge National Laboratory, Oak Ridge, TN, USA. (telephone: 865-574-0355, e-mail: tobinkwjr@ornl.gov).

The coded source imaging (CSI) is a derivative of this technique, when it applies to transmission system, like neutron radiography. Coded source imaging uses a mosaic of pinholes to encode an aperture, thus generating an encoded image of the object at the detector. To reconstruct the image data received by the detector, corresponding decoding patterns are used.

Although requiring post-processing work, coded source imaging is of interest because of its desirable advantages over single pinhole system. CSI system enhances the resolution performance, and maintains sufficient signal-to-noise ratio (SNR). As for the resolution of an imaging system, the L/D ratio is determinant factor, where D is the size of the aperture. The smaller aperture size is, the better resolution can be achieved. However, the transmitted signal will be reduced at the same time. So the aperture size cannot be infinitely small. One way to avoid this is using the coded source. If the coded source is encoded by N pinholes, the L/D ratio of the system is kept as small as that of a single hole, while the SNR is $\sqrt{N}$ times larger.

A coded source imaging system is being installed and tested at the PULSTAR thermal neutron imaging facility. The PULSTAR Reactor at North Carolina State University(NCSU) is a 1 MW pool-type research reactor. It has six beam tubes for extracting radiation for various applications. Beam tube # 5 contains the current thermal neutron imaging collimator system. This collimator is based on a convergent-divergent design, and is equipped with bismuth and sapphire filters that are used to optimize the beam characteristics [1].

An investigation has been initiated to explore the application of coded source imaging techniques at the facility. In this work, Monte Carlo (MCNP) simulations were utilized to explore the needed modifications to the PULSTAR thermal neutron beam to support coded imaging techniques. In addition, an assessment of coded mask design and corresponding correlation reconstruction methods has been performed. The effect of the anti-aperture on reducing the noise in the reconstructed images is also presented. A test experiment using a URA gadolinium mask has been conducted and the point spread function of the system has been measured.

II. CODED SOURCE IMAGING

A. Theory

Similar to conventional neutron radiography, the coded source imaging system involves three principal components – a coded neutron beam, an object, and record devices, which are

represented by three parallel planes in Fig.1. (η,ξ), (u,v), and (x,y).
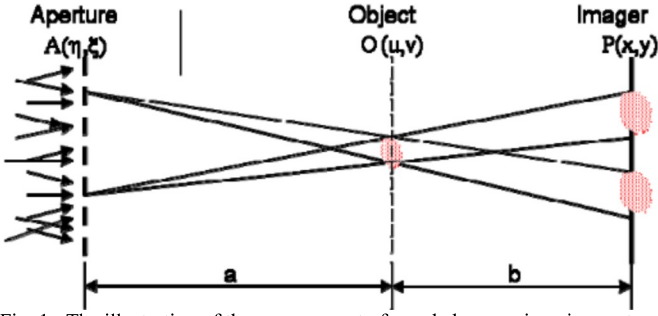

Fig. 1. The illustration of the arrangement of a coded source imaging system.

In the aperture plane, a mosaic of pinholes is used to encode an aperture (or mask). A neutron beam passes through it and forms multiple point sources with a certain pattern. $A(\eta,\xi)$ described the aperture as a function of spatial coordinates. The object plane is relevant to the object to be imaged, the spatial distribution of which is expressed as O(u,v). The imaging plane is relevant to the imaging detectors, where an encoded picture of the object is generated. Each point source in the aperture forms an image in the picture. P(x,y) gives the spatial distribution of the radiation incident on the imaging plane, which should be overlapping images of the object.

The relationship between the aperture, the object and the image can be described as:

$$P(x,y) = \int A(\eta,\xi)O(u,v)dudv$$
$$= \int A(u - \frac{a(x-u)}{b}, v - \frac{a(y-v)}{b})O(u,v)dudv \quad (1)$$

where 'a' is the distance between the aperture and the object, and 'b' is the distance between the object and the imager. It can be recognized in the form of a correlation.

$$P = A * O \quad (2)$$

where '*' is the correlation operator, and A and O represent the aperture and the object.

To reconstruct the image data received by the detector, corresponding decoding patterns are used. In the correlation technique, the reconstructed object is

$$\hat{O} = P * G = RO * (A * G) + N * G \quad (3)$$

where R is the reflection operator, N represents the noise. G is called the post-processing (decoding) array. If A*G is the delta function, the reconstructed imaging will be the object plus a noise term.

The aperture is a binary array, composed of ones and zeros, where the ones in the array represent the pinhole in the aperture, and the zeros represent the opaque. In determining the aperture pattern, uniformly redundant arrays (URAs) are chosen because they have autocorrelation functions with flat side lobes, which is similar to the property of a true delta function. So the reconstructed object of a URA mask has low inherent noise and no limit on the obtainable SNR [2]. The URA array has a dimension of 'r' by 's', both of which are prime numbers, and r-s=2. Moreover, they follow the pattern as

$$A(I,J) = 0 \text{ if I=0,}$$
$$1 \text{ if J=0, I} \neq 0$$
$$1 \text{ if } C_r(I)C_s(J)J=1 \quad (4)$$
$$0 \text{ otherwise}$$

where

$$C_r(I) = 1 \quad \text{if } \exists \text{ an integer x, } 1 \leq x < r,$$
$$\text{and I} = \text{mod}_r x^2 \quad (5)$$
$$0 \quad \text{otherwise}$$

The array 'A' given by Eq.(4) is called the basic array. In order to maintain the delta function nature of A * G, A should have infinite repetitions of the basic array. In practice, as an approximation in a limited space, the basic array is only extended for finite durations in all directions. The most effective mask pattern has the dimension of 2r × 2s, with the basic array in the center.

The post-processing array is given by

$$G(i,j) = G(I,J) \quad (6)$$

where I = mod_ri, J = mod_sj, and

$$G(I,J) = 1 \quad \text{if } A(I,J) = 1$$
$$-1 \quad \text{if } A(I,J) = 0 \quad (7)$$

In practice, the digital imaging process is applied, and the correlation between P and G is quantized. The matrix P is the picture received by the imager, and μ is the pixel size of the image. Matrices A and G should be refined to a smaller scale such that each element corresponds to a physical size of μa/b.

The reconstructed object is formed by

$$\hat{O} = \sum_i \sum_j P(i,j)G(i+k, j+l) \quad (8)$$

Systematic noise can be removed by utilizing the aperture/anti-aperture method. The techniques involves taking two images of the object prior to reconstruction with aperture A^+ and the anti-aperture A^- under the same condition. The aperture A^+ is the same A, which can be generated by the above algorithm. The anti-aperture A^- is formed by

$$A^-(i,j) = 1 \quad \text{if } A^+(i,j) = 0$$
$$0 \quad \text{if } A^+(i,j) = 1 \quad (9)$$

Both G^+ and G^- are created by Eq.(6). Therefore, $G^+ = G^-$. From Eq.(3), we know

$$\hat{O}^+ = P^+ * G^+ = RO * (A^+ * G^+) + N * G^+$$
$$\hat{O}^- = P^- * G^- = RO * (A^- * G^-) + N * G^-$$

By adding two equations together, the noise terms can be cancelled out. And the reconstructed object is given by

$$\hat{O} = \frac{\hat{O}^+ + \hat{O}^-}{2} = \frac{1}{2}[RO * (A^+ * G^+) + RO * (A^- * G^-)] \quad (10)$$

B. *System Design*

The optimized design of coded masks is critical for the performance of this technique and will depend on the characteristics of the imaging beam. The initial design of the imaging beam includes a 1.56 inch × 1.56 inch aperture. Since the beam tube has a direct view towards the reactor core, a 4 inch long polycrystalline bismuth filter (composed of large

monocrystals) is used as a gamma-ray filter and a 6 inch long sapphire single crystal is used as fast neutron filter [3].

In the coded source application, the thermal neutron transmission will be largely reduced compared to the initial design. To enhance the thermal neutron flux, the beam modifications are needed. Fig. 2 shows the simulated neutron energy spectrum at the beam line entrance. The dotted lines are the cross section of Sapphire and Bismuth crystals. The PULSTAR's thermal neutron peak in the spectrum is aligned with the thermal neutron cross section window of Sapphire, but is mismatched with the one of Bismuth. Although bismuth can filter out gamma rays efficiently, it also largely reduces the beam's thermal neutron content. Therefore, MCNP simulations were performed to investigate replacing the bismuth filter with additional sapphire.
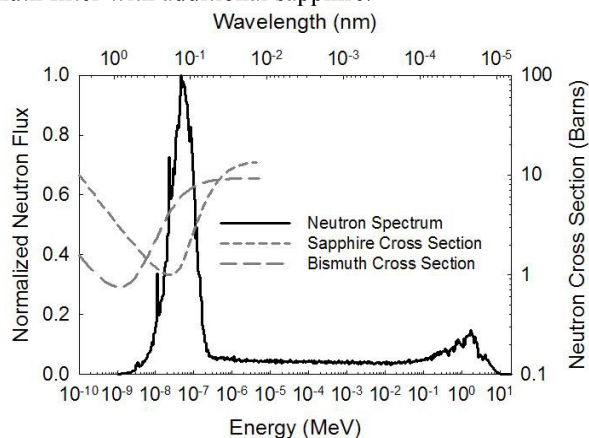

Fig. 2. The solid line shows the simulated neutron energy spectrum at the beam entrance. The dotted lines are cross sections of single crystal Sapphire and Bismuth.

Table 1 gives the details of the beam characteristics with the modified filtration. The 12 inch sapphire produces a nearly 40% increase in the thermal neutron flux, while maintaining a neutron-to-gamma ratio greater than 50. This represents an increase in the gamma contamination of the beam. However, this approach may be acceptable if imaging detectors that are less sensitive to gamma-rays are utilized. Therefore, a beam based on this filter is used in the design of the coded mask.

TABLE I. IMAGING BEAM CHARACTERISTICS FOR DIFFERENT LENGTH SAPPHIRE FILTERS

Filtration	Φ_γ (n·cm^{-3}·sec^{-1})	Φ_γ (n·cm^{-3}·sec^{-1})	N/G	TNC
6 inch sapphire	9.46×10^5	7.72×10^6	8.15	0.986
9 inch sapphire	2.78×10^5	5.95×10^6	21.4	0.997
12 inch sapphire	9.08×10^4	4.78×10^6	52.6	0.999
4 inch bismuth+ 6 inch sapphire	1.19×10^4	3.45×10^6	291	0.996

*TNC is the thermal neutron content, i.e., the ratio of the neutron flux below 0.3eV to the total flux

In order to get the correct reconstructed image, the coded aperture pattern and the corresponding decoding array should be carefully designed, in terms of material thickness and the pinhole morphology. Because of the collimation effect, the mask thickness should be reduced as much as possible, thus a high neutron absorption material is preferred. Gadolinium is

chosen because it has the highest thermal neutron capture cross-section among all the stable material.

Physically, the coded aperture is designed to be distributed in the middle of a 4.2 cm × 4.2 cm square Gadolinium (Gd) sheet. The aperture has a dimension of 38 × 34, which is generated by Eq.(4) and (5), with r=19 and s=17. Each array elements are represented by a square with a side length of 0.1 cm. The pinholes are circles centered in the element, with a diameter of 0.07 cm. Fig. 3 is the picture of a coded aperture fabricated on a Gd sheet. As designed, this aperture contains a total of 648 pinholes out of 1294 elements. The open area fraction is approximately 10%.
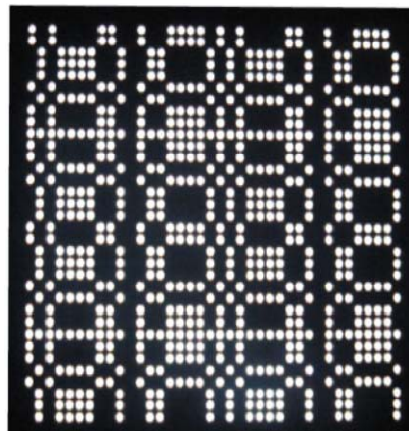

Fig. 3. A 38 by 34 coded aperture fabricated on a 500 μm thick solid Gd sheet.

To study the thermal neutron transmission performance of this aperture, a 400 × 400 point detector array was constructed in MCNP. The total size of the array is 5 cm × 5 cm which provides a pixel size of 125 μm. Two simulations were performed with this model. In the first case, a solid Gd sheet (i.e., without pinholes) was placed on the mask holder (Case 1, Fig. 4a). In the second case, the coded aperture with the above pattern was constructed on the Gd sheet (Case 2, Fig. 4b).
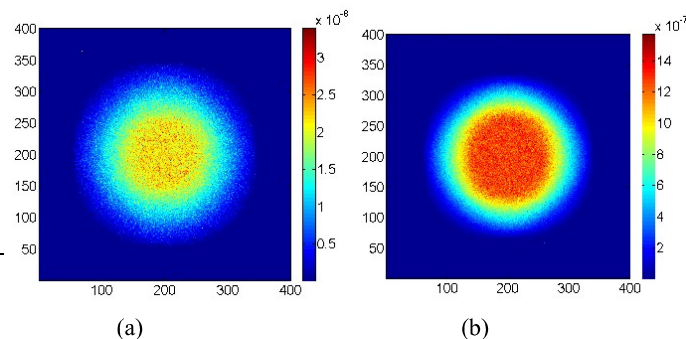

(a)   (b)

Fig. 4. (a) The neutron flux distribution over a 5 cm × 5 cm area using the 500 μm Gd sheet without pinholes (Case 1), (b) The neutron flux distribution over a 5 cm × 5 cm area using the 500 μm Gd aperture with pinhole (Case 2).

Table II lists the transmitted flux in each case and their ratio for different Gd thickness. For a 500μm thick Gd, the ratio of the flux for Case 2 relative to Case 1 was found to be nearly 40. Further increase of the Gd thickness did not change this ratio significantly, which indicates that the detected signal is mainly due to neutrons transmitted through the holes of the mask as opposed to transmission through the Gd itself.

Consequently, a 500 µm thick Gd mask using the coding scheme illustrated in Fig. 3 is machined and has been implemented in imaging experiments at the NCSU PULSTAR reactor.

Gd Thickness (µm)	Φ_1 (n·cm^{-2}·sec^{-1})	Φ_2 (n·cm^{-2}·sec^{-1})	Φ_2/Φ_1
100	1.89×10^{-4}	3.29×10^{-3}	17.4
200	1.07×10^{-4}	3.22×10^{-3}	30.1
300	9.04×10^{-5}	3.19×10^{-3}	35.3
400	8.25×10^{-5}	3.18×10^{-3}	38.5
450	8.05×10^{-5}	3.16×10^{-3}	39.3
500	7.89×10^{-5}	3.16×10^{-3}	40.1
600	7.65×10^{-5}	3.15×10^{-3}	41.2
700	7.46×10^{-5}	3.14×10^{-3}	42.0
800	7.32×10^{-5}	3.13×10^{-3}	42.7
900	7.19×10^{-5}	3.11×10^{-3}	43.3

C. Monte Carlo (MCNP) Simulation

Simulations of neutron radiographs were performed to demonstrate the feasibility of correlation reconstruction method in Eq.(9). The neutron source used in the simulation has an energy distribution shown in Fig. 2. The total neutron flux is measured as $\sim 2.5 \times 10^{12}$ n/cm^2. The gamma source has an energy distribution in Fig.5. The total gamma flux is $\sim 5 \times 10^{14}$ γ/cm^2.
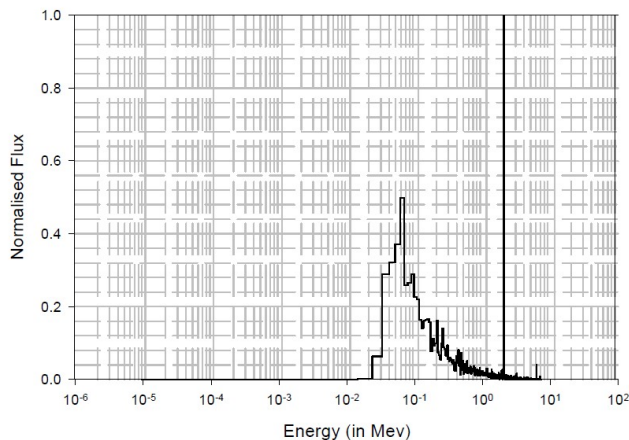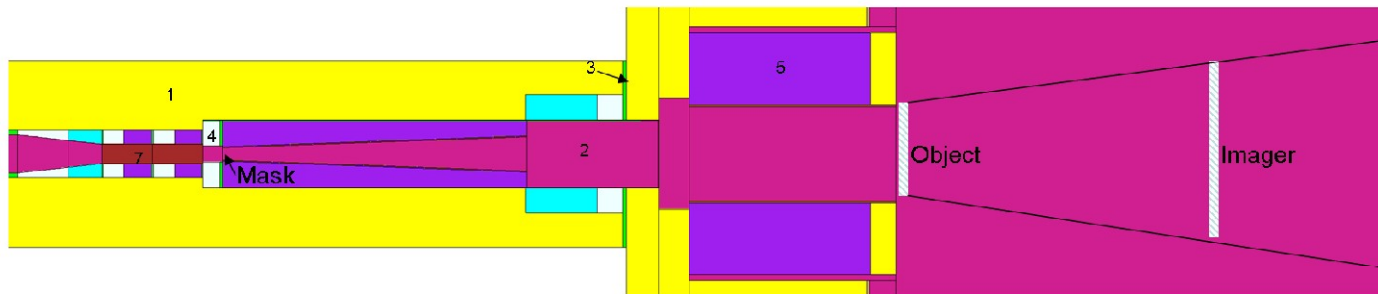
Fig. 5. The simulated gamma energy spectrum at the beam entrance.

Fig. 6 is the sketch of the experimental set-up. The neutron and gamma sources are located at the left side of the system. The planes of mask, object and imager are marked in the figure. The neutrons are first tailored by the convergent collimator and the sapphire filter. After encoded by the mask and adjusted by a divergent collimator, the neutrons will deposit multiple shadows of the object on the imager. An array of point detectors with a grid resolution of 100 µm is used to simulate the performance of an imager. The efficiencies of the imager to neutron and gamma are assumed to be 1 and 0.1.
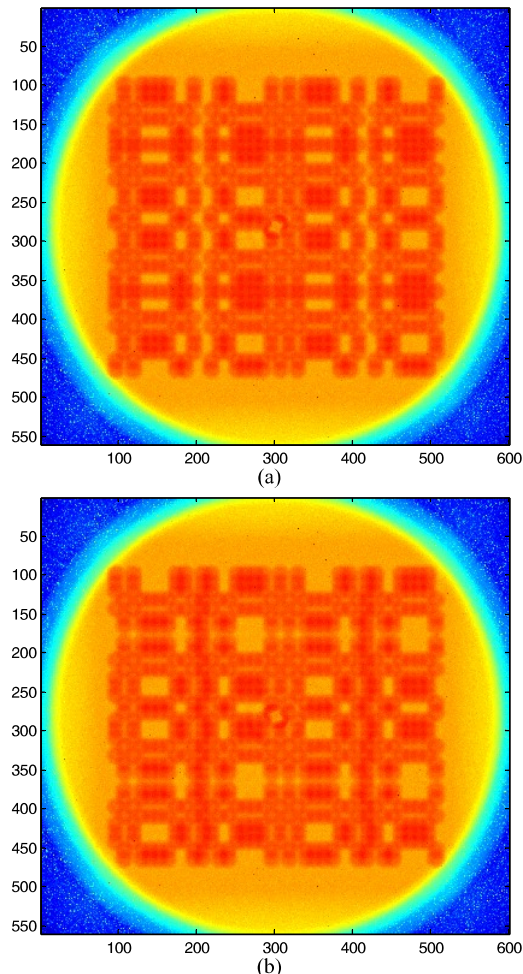
Fig.7. (a) The simulated image of a 1mm diameter pinhole taken with the aperture, (b) The simulated image of a 1mm diameter pinhole taken with the anti-aperture. Both images are shown in log scale.

1. Concrete 2. Air 3. Aluminum 4. Lead 5. RX-277 6. Borated Polyethylene 7. Bismuth Filter

Fig.6. A sketch of the experimental set-up of the coded source system in PULSTAR neutron imaging facility

Fig. 7(a) is the simulated image of a 1mm diameter pinhole taken with the aperture. The systematic noise is introduced because the source in this simulation includes both neutrons and gamma-rays. Fig. 7(b) is the simulated image collected under the same condition, except that the aperture is replaced by the anti-aperture.

The reconstruction in Eq.(8) is applied for different images. Fig. 8(a) shows the reconstructed object from the aperture image, without the gamma background noise imposed on it. The intensity of the noise around the peak is equal to 1.35×10^{15}. Fig. 8(b) shows the reconstructed object from the aperture image, with the gamma noise. The intensity of the noise around the peak is equal to 9.49×10^{15}. In Fig. 8(c), reconstruction is applied to both aperture and anti-aperture images, with gamma noise. Eq.(10) is used to generate the final decoding image. The intensity of noise is reduced to 2.70×10^{15}. This illustrates the obvious effect of the anti-aperture on reducing the noise in the reconstructed images.
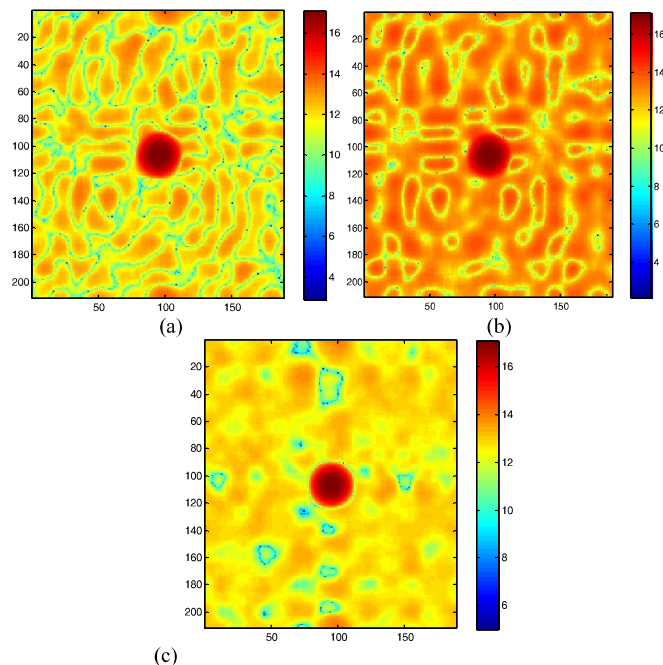

(a)

(b)

(c)

Fig. 8. (a) The reconstructed object from the aperture image without noise. (b) The reconstructed object from the aperture image with noise. (c) The reconstructed object from the aperture/anti-aperture image with noise. The noise term is significantly reduced. All images are plotted in log scale.

The resolution of the coded source imaging system is limited by the pinhole size in the mask. The full-width at half maximum (FWHM) of the point spread function is also studied using the MCNP simulations with the same set-up in Fig. 6. A two-pinhole object, shown in Fig. 9(b), is used in this case. Each of the pinhole has a diameter of 1mm, and the centers are 2mm away from each other. Fig. 9(a) is the picture collected by an array of point detectors at the image plane. Fig. 9(c) shows the decoded image. In the reconstructed object, two peaks are 29 pixels away, corresponding to 2mm in the real object, which determines the pixel size to be 70.0 µm. For both peaks, the FWHM are 14 pixels, i.e. 0.96 mm. This is about the same as the distance between the two closest pinholes in the aperture.
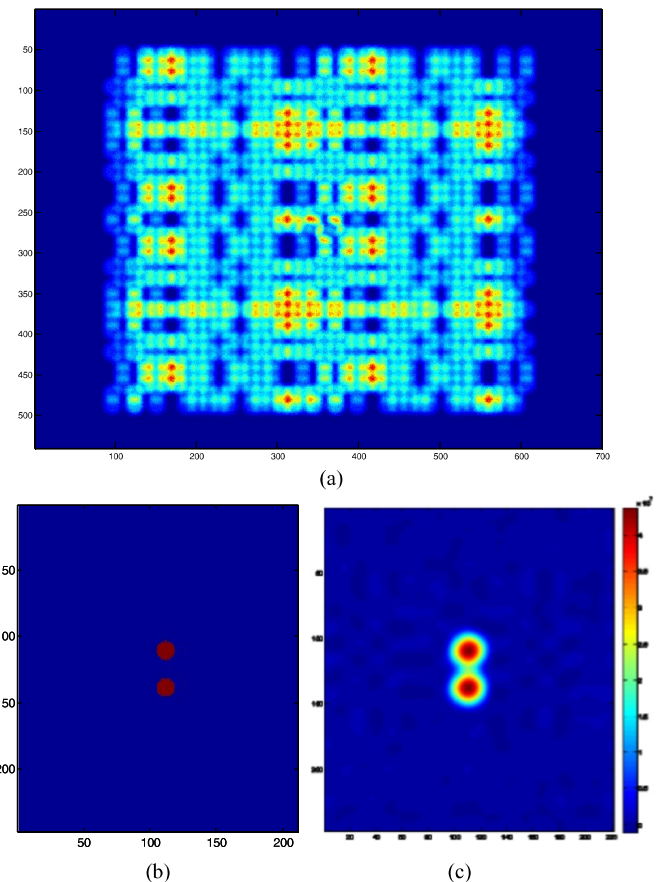

(a)

(b)

(c)

Fig. 9. (a) The image generated by MCNP simulation, of the two-pinhole object (b), the diameter of each hole is 1mm, and the centers are parted 2mm. (c) the reconstructed object from the simulated image

III. EXPERIMENTAL IMPLEMENTATION

A demonstration experiment of the coded source system has been conducted. Two pieces of 6-inch long single crystal sapphire were used as the neutron filter. A coded aperture with 38×34 URA pattern was constructed from a 500 µm thick Gadolinium sheet. The mask has a physical size of 3.8 cm × 3.4 cm. As an object, a 0.25mm thick Cd foil with a 1mm diameter pinhole in the center is attached at the beam exit, which provides a thermal neutron transmission fraction about 1%. The image was taken with a Fuji BAS-NDG Image Plate.

The arrangement is the same as the simulation model in Fig. 6. The distance between the aperture and the object 'a' is 215cm. The distance between the object and the imager 'b' is 224cm. The geometric object magnification in the image plane is $M = (a+b)/a = 2.04$. The resolution of the Image Plate is 100µm. Ideally, the best resolution that can be achieved by this set-up is 50µm. But the resolution of the system is also limited by the size of the pinhole in the aperture. So it cannot exceed 700µm. The field of view is determined by 'a', 'b' and the size of the aperture. In order to reconstruct, the shadows deposited by the pinholes in the diagonal corners of the aperture should not overlap with each other. Therefore, the field of view is within the circle of 1.30cm in radius.

Fig. 10(a) is the recoded picture taken by the Image Plate, and has been processed by spike noise filter and median noise reduction. After background subtraction and decoding, the

reconstructed object is shown in Fig. 10(c). The spread of the peak is due to the size and deformation of the pinhole in the mask. The noise in the surrounding opaque area is a combination of the background noise term N*G and the inherent noise of the system, such as the rotation angle in the recorded images and the manufacturing errors of the mask.

(a)

(b)   (c)

Fig. 10. (a) The recoded picture taken by a Fuji BAS-NDG neutron sensitive Image Plate, (b) the 1mm diameter pinhole in a Cd sheet, used as an object, (c) the reconstructed object from the recorded picture.

IV. CONCLUSION

A coded source imaging system is being installed and tested at the PULSTAR reactor neutron imaging facility. A 12 inch single crystal sapphire filter was found to produce the optimum thermal neutron beam for such a system. A coded mask with a URA pattern was fabricated on a 500μm Gd sheet. A demonstration experiment has been conducted with the optimized beam line. The point spread function of the system was measured. MCNP simulations show that the aperture/anti-aperture method will reduce the systematic noise in the reconstructed image significantly. Currently, a corresponding anti-aperture has been machined, and the performance of this method is being examined.

REFERENCES

[1]   K. K. Mishra, A. I. Hawari, and V. H. Gillette, "Design and Performance of a Thermal Neutron Imaging Facility at the North Carolina State University PULSTAR Reactor," *IEEE Trans. Nucl. Sci*, vol. 53, no. 6, pp. 3904-3911, 2006.

[2]   E. Fenimore, T. Cannon, "Coded Aperture Imaging with Uniformly Redundant Arrays," *Appl. Opt.* Vol. 17, pp. 337-347, 1978.

[3]   A. I. Hawari, I. I. Al-Qasir, and K. K. Mishra, "Accurate simulation of thermal neutron filter effects in the design of research reactor beam applications," proceedings of *PHYSOR-2006: Advances in Nuclear Analysis and Simul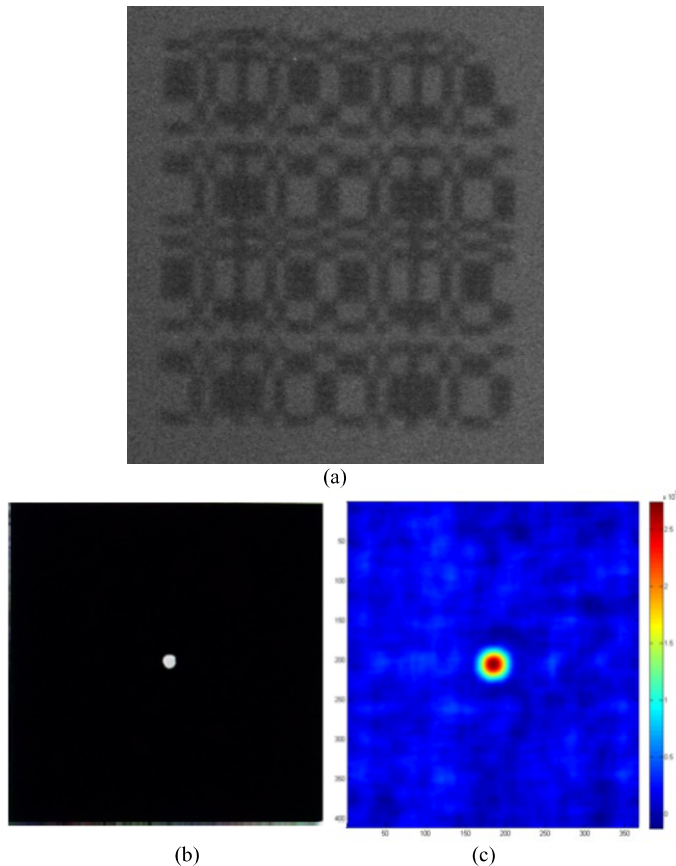ation*, Vancouver, Canada, 2006.